*Textures and Microstructures*, 1986, Vol. 6, pp. 289–313
0730–3300/86/0604–0289 $18.50/0

Printed in the United Kingdom

# Determination of the Complete Orientation Distribution Function by the Zero-Range Method

H. P. LEE,† H. J. BUNGE† and C. ESLING‡

† *Institut für Metallkunde und Metallphysik, TU Clausthal, Germany*
‡ *Laboratoire de Métallurgie Structurale, Université de Metz, France*

(*Received May 3 1986*)

Because of the superposition of pole figures corresponding to symmetrically equivalent crystal directions, only the reduced orientation distribution function $\tilde{f}(g)$ can be obtained directly by pole figure inversion. The additional information contained in the positivity condition of the ODF allows, however, the determination of an approximation to the "indeterminable" part and hence of the complete ODF $f(g)$, if the texture has sufficiently large zero-ranges. The application of the method and the accuracy of the results was tested using two theoretical and one experimental textures. The accuracy of the complete ODF depends on the size of the zero-range, the errors in its determination, and on the errors, experimental and truncational, of the reduced ODF. The "physical zero" used in order to determine the zero-range is defined according to the statistical error of the pole figure measurement.

## INTRODUCTION

Single phase polycrystalline materials consist of crystallites of the same crystal structure but with different orientations of their crystal axes with respect to a sample fixed coordinate system as is shown in Figure 1. The relative frequency of the material having on orientation $g$ within the orientation range $dg$ is given by the orientation

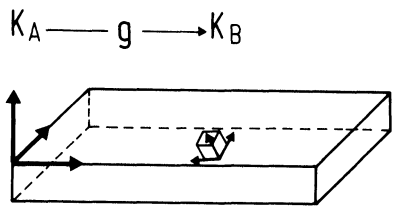


FIGURE 1 Definition of the crystal orientation $g$ by a sample coordinate system $K_A$ and a crystal coordinate system $K_B$.

distribution function $f(g)$

$$\frac{dV}{V} = f(g)\, dg, \qquad g = \{\varphi_1, \phi, \varphi_2\} \tag{1}$$

The orientation $g$ is described by three orientation parameters which may be the Euler angles given in Eq. (1). The orientation distribution function (ODF), especially if it is not the statistically random distribution, is called the *texture* of the material.

There are principally two different ways how to determine the texture, these are:

1). Single orientation measurements,

2). Pole figure measurements.

In the first case the orientations of a large number of crystallites have to be determined. This can be done by diffraction methods such as Laue photographs or Kikuchi patterns, or by optical methods. In optically biaxial materials it is, in principle, possible to obtain the complete crystal orientation by polarized light microscopy either in the transmission or in the back-reflection case. Optically uniaxial materials allow only the orientation of the optical axis to be obtained by these methods. In the optically isotropic cubic metals this method cannot be applied. Single orientation measurements are, however, possible also in this case using the traces of certain crystallographic planes in a metallographic section such as for instance etch pits, twin-lamellae, and the like.

The primary result of a single orientation texture determination is a "cloud" of orientation points $g$ of the crystallites represented in the space of the Euler angles $\varphi_1$, $\phi$, $\varphi_2$ (Wenk and Wilde, 1972).

The orientation density can then be constructed by counting the number of points $\Delta N$ within each volume element $\Delta g$ in the orientation space and interpolating the so obtained values of the orientation density by a continuous function $f(g)$ according to Eq. (1). The statistical error of this method

$$\frac{\Delta f}{f} = (N \cdot f(g) \cdot \Delta g)^{-1/2} \tag{2}$$

depends on the total number $N$ of measured crystal orientations and on the angular resolving power $\Delta g$. Hence, in order to obtain a statistically relevant distribution function $f(g)$ with a sufficiently high angular resolving power, it is necessary to measure a great number, e.g. some hundreds, of orientations. This method is thus tedious and time consuming. It can only be used in certain special cases. It is, however, to be mentioned that it gives directly the "complete" ODF, $f(g)$ according to the definition of Eq. (1) which is generally not the case in the pole figure method.

## TEXTURE DETERMINATION BY POLE FIGURE INVERSION

In the second method which is used in the great majority of texture determinations, so called pole figures are measured (Wassermann and Grewen, 1962). These are *direction* distribution functions of specific crystal directions $h$, the normal directions to reflecting lattice planes $(hkl)$

$$\frac{dV}{V} = P_h(y)\, dy, \qquad y = \{\alpha, \beta\} \tag{3}$$

where the orientation of the crystal direction $h$ with respect to the sample coordinate system is described by two orientation parameters which may be the spherical polar coordinates $\alpha, \beta$ as was assumed in Eq. (3). Pole figures are two-dimensional distribution functions. A possible rotation of the crystallites about the direction $h$ remains, in this case, undetected. A pole figure is thus a two-dimensional "projection" of the three-dimensional orientation

distribution function $f(g)$ related to the latter one by the integral

$$P_h(y) = \frac{1}{2\pi} \int_{h \| y} f(g)\, d\gamma \tag{4}$$

which is to be taken over all those orientations for which the crystal direction $h$ is parallel to the sample direction $y = \{\alpha, \beta\}$, and the angle $\gamma$ describes a rotation about this direction (ref. e.g. Bunge 1982).

Equation (4) can be solved for $f(g)$ *exactly* if the pole figures of all crystal directions $h$ are known. This procedure has been called *pole figure inversion.* Four different methods of pole figure inversion have been proposed thus far. These are:

1) The discretization method (vector method) (Williams, 1968 and Ruer and Baro, 1977)

2) The series expansion method (harmonic method) (Bunge, 1965 and Roe, 1965)

3) The probabilistic method (Imhof, 1977)

4) The integral transformation method (inversion formula) (Matthies, 1979)

Each of these methods has its specific advantages and disadvantages but in principle they all provide the complete solution to Eq. (4) which is unique if the pole figures are known for all crystal directions $h$, i.e. as a continuous function of $h$ covering the total solid angular range $4\pi$ (Esling and Bunge, 1981).

If only a finite number of pole figures are known, e.g. those, the directions $h$ of which are normal directions to low-index lattice planes, then only an approximation to $f(g)$ can be obtained which is generally not unique. The ambiguity of the solution, in this case, is independent of the specific method used to solve Eq. (4). This implies of course that each method may yield another specific solution to Eq. (4) within the ambiguity range.

## SYMMETRICALLY SUPERPOSED POLE FIGURES

The crystals may have a certain crystal symmetry $G^c$ with the symmetry operations $o^c$ which can be pure rotations $g^c$ or rotational

inversions $u^c$

$$G^c = \{o^c\} = \{g^c, u^c\} \tag{5}$$

The application of the symmetry operations to the crystal direction $h$ yields a set of symmetrically equivalent directions $\{h\}$, the pole figures of which cannot be measured separately by polycrystal X-ray diffraction. Hence, only the superposed pole figure

$$\tilde{P}_{\{h\}}(y) = \frac{1}{N^c} \sum_{G^c} P_{o^c \cdot h}(y) \tag{6}$$

can be measured where $N^c$ is the order of the symmetry group $G^c$.

The orientation distribution function $f(g)$ can be constructed such that it is invariant with respect to all crystal symmetry *rotations* $g^c$

$$f(g^c \cdot g) = f(g) \tag{7}$$

Hence, these symmetries need not be further considered in Eq. (6). The inversion elements $u^c$ can be expressed as the product of one out of them $u^{c_1}$ (the generating element) and all the rotations $g^c$

$$u^c = u^{c_1} \cdot g^c \tag{8}$$

Hence, it turns out that in Eq. (6) only the generating symmetry operation (of second kind) has to be considered. Equation (6) then reads

$$\tilde{P}_{\{h\}}(y) = \tfrac{1}{2}[P_h(y) + P_{u^{c_1} \cdot h}(y)] \tag{9}$$

It further turns out that it is always possible to choose the generating element $u^{c_1}$ out of the three operations (Bunge, Esling and Müller, 1980, 1981).

$$u^{c_1} = \{\bar{1} = i, \bar{2} = m, \bar{4}\} \tag{10}$$

The most important one of which is the inversion centre $\bar{1}$ (Matthies, 1979).

If pole figure measurements are being carried out by normal diffraction experiments then Friedel's law holds which adds an inversion centre to the crystal symmetry. Hence, with normal scattering, the generating element $u^{c_1}$ is always the inversion centre $\bar{1}$ independent of the true crystal symmetry. The two cases $\bar{2}$ and $\bar{4}$ can only be observed when using anomalous scattering in which case Friedel's law does not hold generally (Bunge and Esling, 1981).

In the case of centro-symmetry (either by the crystal symmetry itself or by virtue of Friedel's law) Eq. (9) takes on the form

$$\tilde{P}_{\{h\}}(y) = \tfrac{1}{2}[P_h(y) + P_{-h}(y)] \tag{11}$$

Eq. (4) has thus to be replaced by

$$\tilde{P}_{\{h\}}(y) = \frac{1}{2\pi} \int_{\pm h \| y} f(g)\, d\gamma \tag{12}$$

which has *no unique solution.* The complete ODF, i.e. the solution of Eq. (4) is also a solution of Eq. (12) which can be written

$$f(g) = \tilde{f}(g) + \tilde{\tilde{f}}(g) \geq 0 \tag{13}$$

where $\tilde{\tilde{f}}(g)$ is called the "indeterminable" part. $\tilde{\tilde{f}}(g)$ is the kernel of the "projection operator", Eq. (12), which projects the three-dimensional function $f(g)$ into the superposed pole figure $\tilde{P}_{\{h\}}(y)$. The kernel is thereby projected into zero. Hence, $\tilde{\tilde{f}}(g)$ can be changed deliberately without changing the measured pole figure $\tilde{P}_{\{h\}}(y)$. This is meant when we call $\tilde{\tilde{f}}(g)$ the "indeterminable" part of the ODF.

It is also to be mentioned, that the splitting of an orientation distribution function $f(g)$ into the two parts $\tilde{f}(g)$ and $\tilde{\tilde{f}}(g)$, Eq. (13), is always unique. In this sense $\tilde{f}(g)$, the so called determinable part of the ODF or the reduced ODF is a unique solution of Eq. (12) (Matthies, 1979),

The superposition Eq. (9) does not occur, of course, in polycrystals belonging to an enantiomorphic class which does not contain symmetry operations $u^c$ of the second kind. In this case, however, right-handed and left-handed crystal forms may occur with the volume fractions $M^R$ and $M^L$. The two kinds of crystals may have different textures. Hence, in this case too superposed pole figures occur (Bunge and Esling, 1985)

$$\tilde{P}_{\{h\}}(y) = M^R P_h^R(y) + M^L P_h^L(y) \tag{14}$$

Hence, also in this case it is not possible to determine the true ODFs of the two crystal forms i.e. $f^R(g)$ and $f^L(g)$ from the experimentally measured pole figures completely.

There is only one case in which the true ODF can be obtained directly by pole figure inversion. This is the case of enantiomorphic crystals, the polycrystal of which contains only one form, say the

right-handed one

$$M^R = 1, \qquad M^L = 0 \tag{15}$$

In this case it is

$$\tilde{P}_{\{h\}}(y) = P_h^R(y) \tag{16}$$

and the inversion process yields the complete ODF with no indeterminable kernel. In this case, pole figure measurement has to be carried out using anomalous scattering.

## DETERMINATION OF AN APPROXIMATION TO $\tilde{\tilde{f}}(g)$ BY THE ZERO-RANGE METHOD

An approximation to $\tilde{\tilde{f}}(g)$ can be obtained in certain cases using the additional information contained in the positivity of Eq. (13). Because of the positivity condition (and only by this condition) the variability range of $\tilde{\tilde{f}}(g)$ is restricted. The restriction turns to complete determination in the zero-range $Z^0$ of $f(g)$ which is defined by

$$f(g^0) = 0, \qquad g^0 \text{ in } Z^0 \tag{17}$$

In the zero-ranges it is

$$\tilde{\tilde{f}}(g) = -\tilde{f}(g) \tag{18}$$

Since $\tilde{f}(g)$ is known by pole figure inversion from $\tilde{P}_{\{h\}}$, Eq. (12), also $\tilde{\tilde{f}}(g)$ is known in $Z^0$. It may thus be approximated by an approximation function $\tilde{\tilde{f}}_{L_1}(g)$ of an appropriate order using a minimum deviation condition in $Z^0$ such that

$$\int_{Z^0} [\tilde{\tilde{f}}(g) - \tilde{\tilde{f}}_{L_1}(g)]^2 \, dg = \text{Min} \tag{19}$$

While $\tilde{\tilde{f}}(g)$ is known, according to Eq. (18), only in $Z^0$ but not outside, the approximation function $\tilde{\tilde{f}}_{L_1}(g)$ is defined in the whole orientation space. An approximation to the complete ODF $f(g)$ in the non-zero-range is thus given by

$$f_{LL_1}(g) = \tilde{f}_L(g) + \tilde{\tilde{f}}_{L_1}(g) \tag{20}$$

as is shown schematically in Figure 2.

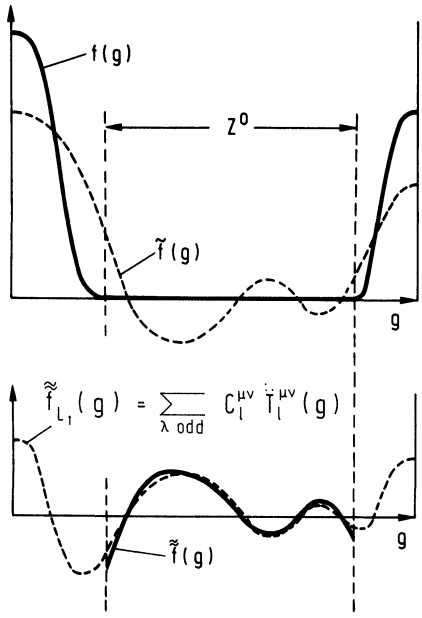


FIGURE 2 Approximation of $\tilde{\tilde{f}}(g)$ in the zero-range and extrapolation of this function into the non-zero-range.

A convenient way (but not the only one) of defining an approximation function is to use a series approximation (Bunge and Esling, 1979)

$$\tilde{f}_L(g) = \sum_{\lambda=\text{even}}^{L} \sum_{\mu=1}^{M(l)} \sum_{\nu=1}^{N(l)} C_l^{\mu\nu} \ddot{T}_l^{\mu\nu}(g)$$
$$\tilde{\tilde{f}}_{L_1}(g) = \sum_{\lambda=\text{odd}}^{L_1} \sum_{\mu=1}^{M(l)} \sum_{\nu=1}^{N(l)} C_l^{\mu\nu} \ddot{T}_l^{\mu\nu}(g) \tag{21}$$

where $\ddot{T}_l^{\mu\nu}$ are generalized spherical harmonics which are invariant with respect to symmetry rotations of the crystal and sample symmetry. The summation in Eq. (21) is carried out over even or odd values of the index $\lambda$ respectively, whereby $\lambda$ is defined in a different way according to the three cases distinguished in Eq. (10).

It is (Bunge and Esling, 1985)

$$\lambda = \begin{cases} = l & \\ = l + m & \text{if } u^{c_1} = \bar{2} \\ = l + m/2 & = \bar{4} \end{cases} \qquad = \bar{1} \tag{22}$$

The most important one of these cases is that of centrosymmetry (Matthies, 1979, 1982). In this case the summation is to be carried out over even and odd values of the index 1 respectively. The other two cases require the use of anomalous scattering in order to avoid Friedel's law (Bunge and Esling, 1981).

The fundamental equation of the zero-range method, Eq. (19), then reads

$$\int_{Z^0} \left[ -\tilde{f}_L(g) - \sum_{\lambda=\text{odd}}^{L_1} \sum_{\mu=1}^{M(l)} \sum_{\nu=1}^{N(l)} C_l^{\mu\nu} \dot{\dot{T}}_l^{\mu\nu}(g) \right]^2 dg = \min \tag{23}$$

Eq. (23) is to be minimized for the coefficients $C_l^{\mu\nu}$. With the abbreviations

$$\int_{Z^0} \dot{\dot{T}}_l^{\mu\nu}(g) \cdot \dot{\dot{T}}_{l'}^{\mu'\nu'}(g)\, dg = \alpha_{ll'}^{\mu\mu'\nu\nu'} \tag{24}$$

$$\int_{Z^0} \tilde{f}_L(g) \cdot \dot{\dot{T}}_l^{\mu\nu}(g)\, dg = a_l^{\mu\nu} \tag{25}$$

this leads to the conditions

$$\sum_{\lambda=\text{odd}}^{L_1} \sum_{\mu=1}^{M(l)} \sum_{\nu=1}^{N(l)} C_l^{\mu\nu} \alpha_{ll'}^{\mu\mu'\nu\nu'} = a_{l'}^{\mu'\nu'} \tag{26}$$

from which the coefficients $C_l^{\mu\nu}$ can be obtained up to $l = L_1$. It is convenient to solve Eq. (26) by an iterative method.

## DEFINITION OF THE ZERO-RANGE

In order to apply the zero-range method, the zero-range $Z^0$ in the orientation space has to be known. This zero-range can be obtained from the zero-ranges in the pole figures in a purely geometrical way without knowing anything else about the pole figures or the ODFs $f(g)$ or $\tilde{f}(g)$. This "mathematical" definition of the zero-range will

be replaced, later on, by a physical definition of "zero" taking the experimental error into account.

## MATHEMATICAL DEFINITION OF THE ZERO-RANGE

The zero-range $Z^0$ in the orientation space can be determined directly from the zero-ranges $z_h^0$ of the superposed experimental pole figures which are defined by

$$\tilde{P}_{\{h\}}(y_h^0) = 0 \qquad y_h^0 \quad \text{in} \quad z_h^0 \tag{27}$$

Since pole densities are not negative it follows from Eq. (6) for each individual pole figure

$$P_{0^{\circ},h}(y_h^0) = 0 \qquad y_h^0 \quad \text{in} \quad z_h^0 \tag{28}$$

i.e. the zero-range of the superposed pole figure is the common part of the zero-ranges of the individual pole figures of all symmetrically equivalent crystal directions. Furthermore, because of the positivity condition Eq. (13) the integrand $f(g)$ in Eq. (4) must be zero in the whole integration interval if the integral $P_h(y)$ is zero. Hence, a *zero-point* in a superposed pole figure Eq. (27) implies a *zero-line* in the orientation space for each of the symmetrically equivalent crystal directions $\{h\}$. If the relation

$$y_h^0 = g^0 \cdot \{h\} \tag{29}$$

is fulfilled for an orientation $g^0$ and anyone of the symmetrically equivalent crystal directions $\{h\}$, i.e. if any of these directions falls into the zero-range $y_h^0$ of the corresponding pole figure, then $g^0$ belongs to the zero-range $Z^0$ in the orientation space. This is a simple geometrical relationship which can easily be tested for each point $g$ of the orientation space. Eq. (29), applied to one set $\{h\}$ of crystal directions, is a sufficient but not necessary condition for a point $g^0$ to be in the zero-range. Other parts of the zero-range may be obtained when Eq. (29) is applied to other pole figures $\{h'\}$. The zero-range is then taken as the enveloppe of the zero-ranges obtained from the individual pole figures as is shown schematically in Fig. 3. It must be mentioned however that, even applied to all pole figures, Eq. (29) is still only a sufficient but not a necessary condition for a point to be in the zero-range. The total zero-range

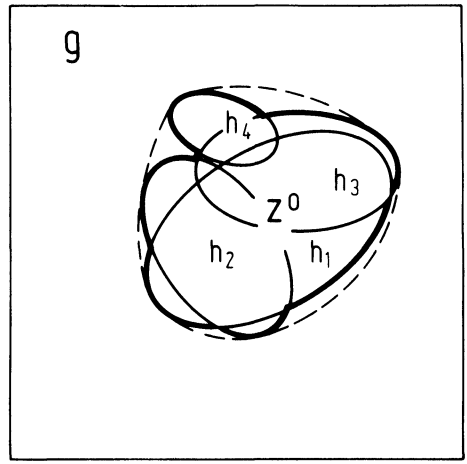


FIGURE 3 The total zero-range $Z^0$ is the envelope of the partial zero-ranges $Z_h^0$ obtained from the zero-range $z_h^0$ in the pole figures.

may thus still be larger than the so obtained envelope. (Bechler-Ferry, Bunge and Esling, 1981).

## PHYSICAL DEFINITION OF THE ZERO-RANGE

Since the pole figures are obtained experimentally, the "mathematical" definition of the "zero" in Eq. (27) has to be replaced by a physical definition of "zero" (Esling, Bechler-Ferry and Bunge, 1981). Usually the pole figures are measured by pulse counting techniques. The pole figure values and their respective errors are then obtained by

$$P = [(N \pm \sqrt{N}) - (N_{\text{back}} \pm \sqrt{N_{\text{back}}})] \cdot n \tag{30}$$

where $N$ is the number of pulses counted in the Bragg-position and $N_{\text{back}}$ is the number of pulses of the background scattering measured in an appropriate off-Bragg-position and $n$ is the normalization factor. The pole figure must be assumed to be "physically" zero if $P$ is in the order of magnitude of its statistical error i.e.

$$P^0_{\text{min}} = 2\sqrt{N_{\text{back}}} \cdot n \tag{31}$$

Eq. (31) can be considered the physical definition of the zero-range (This defines the lower limit of the extension of the zero-range, $Z^0_{\min}$).

It is, however, to be borne in mind that the approximation function $\tilde{\tilde{f}}_{L_1}$ is obtained from the condition Eq. (19) which contains $\tilde{f}(g)$ in the zero-range. But $\tilde{f}(g)$ is obtained from the pole figures by pole figure inversion, i.e. including *all* pole figure values and their respective errors. The absolute values of these errors are highest in the maximum points of the pole figures. Hence, it may be meaningful to admit a deviation from zero in the order of magnitude of the maximum error in the pole figures. A maximum zero-range may thus defined by (Lee, Welch, Esling and Bunge, 1984)

$$P^0_{\max} = \sqrt{N_{\max}} \cdot n \tag{32}$$

where $N_{\max}$ is the maximum number of pulses counted in a pole figure. An optimum definition of "physical" zero may be found somewhere between the maximum value Eq. (32) and the minimum value Eq. (31).

In these considerations it was assumed that the accuracy of pole figure measurements is only limited by the pulse counting statistics and not by other experimental errors. If, for example, the material is coarse grained, then the accuracy may be limited by the number of grains included in the measurement rather than by the number of counted pulses. In this case the maximum value of error in the pole figures may be given by a formula similar to Eq. (2) rather than by Eq. (32).

## DEFINITION OF THE ZERO-RANGE FROM RECALCULATED POLE FIGURES

According to the considerations in the previous section it is meaningful to define the "physical" zero in the pole figures in relation to all errors entering $\tilde{f}(g)$ in Eq. (23). This includes experimental errors, which may be different in different pole figures and in different points of the pole figures and it includes also series truncation errors. The zero-range may thus be meaningfully estim-

ated from pole figures recalculated from the coefficients $C_l^{\mu\nu}$. These recalculated pole figures contain errors which are mean values of the experimental errors of all pole figures and of the series truncation effect. A good estimation of the resulting errors is obtained by the *maximum negative value* in the recalculated pole figures, the absolute value of which is then used as the boundary value of the zero-range $P^0$.

The use of recalculated pole figures for the definition of the zero-range may especially be indicated if the experimental pole figures are incomplete e.g. by using measurements only in the back-reflection range from which only part of the zero-range can be deduced.

## DEFINITION OF THE ZERO-RANGE BY A MINIMIZATION PROCESS

In a preceding section it was discussed that the zero-range has to be defined by a pole figure value which is somewhere in between the minimum value of Eq. (31) and the maximum value of Eq. (32). If the zero-range has been chosen too small then the basis for the calculation of $\tilde{\tilde{f}}_{L_1}$ is too small (see Figure 2). This means the determinant of Eq. (26) is small such that the solution of this equation is uncertain. The uncertainty expresses itself in the number $n$ of cycles to convergence needed in an iterative solution of Eq. (26).

If, on the other hand, the zero-range has been chosen too large, then non-zero-ranges in which Eq. (18) does not hold, are included in the calculation. This gives rise to additional errors in $\tilde{\tilde{f}}_{L_1}$. The accuracy of the solution may be estimated by the negativity ranges of the complete ODF. We define an accuracy parameter

$$r = \int_{Z^-} |f(g)|\, dg \tag{33}$$

where $Z^-$ is the negativity range of $f(g)$. An optimum value of the zero-range can thus be estimated with help of these two criteria (Lee 1985).

## APPLICATION OF THE ZERO-RANGE METHOD

### Theoretical textures

In order to check the zero-range method described above, the method was applied to some theoretical textures consisting of an ideal orientation $g_{\{hkl\}\langle uvw\rangle}$ (and its symmetrical equivalents) with a spread range about it according to a Gauss-distribution. The coefficients $C_l^{\mu\nu}$ of such a texture can be calculated theoretically

$$C_l^{\mu\nu} = \frac{\exp\{-\frac{1}{4}l^2\omega_0^2\} - \exp\{-\frac{1}{4}(l+1)^2\omega_0^2\}}{1-\exp\{-\frac{1}{4}\omega_0^2\}} \cdot \dot{T}_l^{\mu\nu}(g_{\{hkl\}\langle uvw\rangle}) \quad (34)$$

Eq. (34) holds for all orders $l$, especially also for odd values of $l$ in the case of centrosymmetric crystals. From the coefficients $C_l^{\mu\nu}$, Eq. (34), pole figure coefficients $F_l^{\gamma}(h)$ can be obtained and from these coefficients theoretical pole figures can be calculated. If, in this calculation, only the coefficients $F_l^{\gamma}(h)$ of even order $l$ are used then the superposed pole figures according to Eq. (11) are obtained. The zero-range method can then be applied to these pole figures and the so obtained coefficients $C_l^{\mu\nu}$ of odd order $l$ can be compared with the theoretical ones obtained from Eq. (34). This was applied to the orientation $g = \{110\}\langle 112\rangle$ assuming cubic-orthorhombic symmetry and a spread angle $\omega_0 = 12°$ (corresponding to a full-width-half-maximum (FWHM) value of 20°, Lee, 1985). The series expansion was extended to $L = 22$. The so obtained (100) and (111) pole figures are shown in Figure 4. A section at $\alpha = 90°$ of the (111) pole

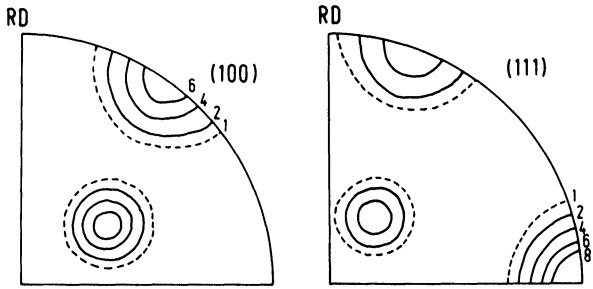


FIGURE 4 Pole figures of an ideal texture $g = \{110\}\langle 112\rangle$ with $\omega_0 = 12°$ calculated with coefficients of even order l according to Eq. (34).

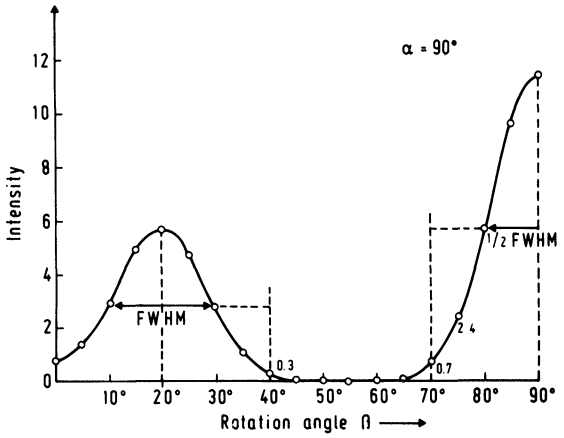


FIGURE 5 The $\alpha = 90°$ section of the (111) pole figure of Figure 4.

figure is shown in Figure 5. It is seen that there is no truncation error within the accuracy of drawing. Since these pole figures are theoretical ones the definition of a "physical" zero value according to Eq. (30) or (31) cannot be applied in this case. Therefore three values

$$P_1^0 = 0.05, \qquad P_2^0 = 0.3, \qquad P_3^0 = 2.0 \tag{35}$$

where chosen arbitrarily. The zero-ranges in the orientation space, obtained with these definitions are shown in Figure 6. Odd coefficients $C_l^{\mu\nu}$ were then obtained by solving Eq. (26) with $L_1 = 21$. The so obtained coefficients for the case $P_1^0$ are compared with the theoretical ones in Table 1. Mean values over $\mu$ and $\nu$ of these coefficients are shown in Figure 7. It is seen that the values for $P_1^0$ are indistinguishable from the theoretical ones within the accuracy of drawing. Also $P_2^0$ gives rise to very small errors. Only $P_3^0$, leading to a too large zero-range, introduces strong errors. Sections through the orientation distribution functions are shown in Figure 8. The function calculated with $P_1^0$ is indistinguishable from the theoretical one within the drawing accuracy. The influence of the definition of the zero-range can also be seen in Figure 9 which shows the negativity values according to Eq. (33) as a function of $P_i^0$.

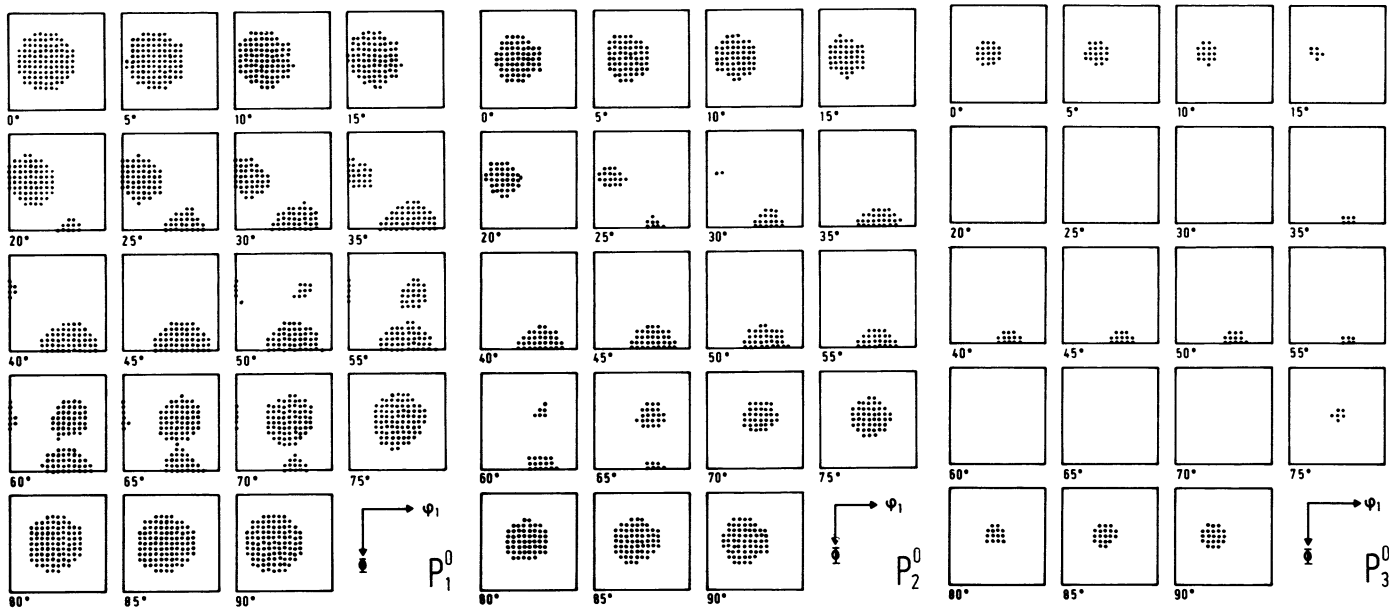


FIGURE 6 Zero-ranges (white) obtained from the pole figures Figure 4 with the three definitions of physical zero according to Eq. (35).

TABLE I

Coefficients $C_l^{\mu\nu}$ of a theoretical texture $g = \{110\}\langle 112\rangle$, $\omega_0 = 12°$. theor.: according to Eq. (34); cal.: according to the zero-range method

| L, μ \ ν | | 2 | 3 | 4 | 5 | 6 | 7 | 8 | 9 | 10 | 11 |
|---|---|---|---|---|---|---|---|---|---|---|---|
| L = 9 | theor. | -1.722 | -0.572 | 2.094 | -0.748 | | | | | | |
| μ = 1 | cal. | -1.730 | -0.578 | 2.093 | -0.750 | | | | | | |
| L = 13 | theor. | 0.278 | -1.872 | 0.557 | 0.269 | 0.976 | -0.892 | | | | |
| μ = 1 | cal. | 0.273 | -1.860 | 0.551 | 0.268 | 0.963 | -0.884 | | | | |
| L = 15 | theor. | -0.484 | -0.498 | -0.293 | 0.009 | 0.647 | 0.547 | -0.594 | | | |
| μ = 1 | cal | -0.471 | -0.493 | -0.290 | 0.007 | 0.629 | 0.534 | -0.578 | | | |
| L = 17 | theor. | -0.121 | 0.254 | 0.579 | 0.047 | -0.535 | -0.008 | -0.323 | 0.421 | | |
| μ = 1 | cal. | -0.127 | 0.254 | 0.574 | 0.042 | -0.541 | 0.006 | -0.323 | 0.419 | | |
| L = 19 | theor. | 0.029 | -0.224 | 0.259 | -0.016 | -0.032 | -0.121 | 0.127 | -0.075 | -0.000 | |
| μ = 1 | cal. | 0.044 | -0.232 | 0.288 | -0.016 | -0.038 | -0.129 | 0.124 | -0.098 | 0.007 | |
| L = 21 | theor. | 0.020 | -0.078 | -0.054 | 0.020 | -0.065 | 0.059 | 0.027 | 0.059 | -0.000 | -0.064 |
| μ = 1 | cal. | 0.033 | -0.076 | -0.074 | 0.019 | -0.087 | 0.077 | 0.025 | 0.062 | 0.012 | -0.074 |
| | theor. | -0.054 | -0.069 | -0.041 | -0.005 | -.0010 | -0.005 | 0.042 | 0.107 | 0.000 | -0.075 |
| μ = 2 | cal. | -0.057 | -0.077 | -0.036 | -0.008 | -0.023 | -0.007 | 0.051 | 0.116 | 0.009 | -0.073 |

Similar calculations were carried out with the same ideal orientation $g = \{110\}\langle 112\rangle$ but with a smaller spread about it, $\omega_0 = 6°$. In this case a truncation error occurs with $L = 22$ in the pole figures as is shown in Figure 10. This truncation error can be assumed as a simulation of the experimental error in pole figures, leading to a corresponding error in the reduced ODF $\tilde{f}(g)$ from which the zero-range method starts. The zero-range was defined according to $P_1^0$ which introduced the smallest error in the preceding calculation

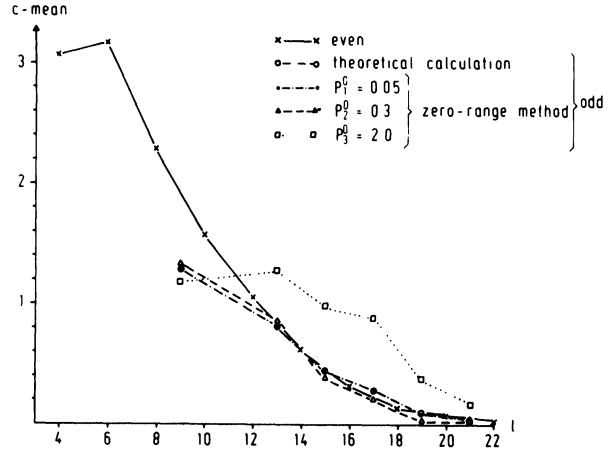


FIGURE 7 Mean values of the coefficients $C_l^{\mu\nu}$ obtained theoretically according to Eq. (34) compared with values obtained by the zero-range method according to the three definitions Eq. (35).

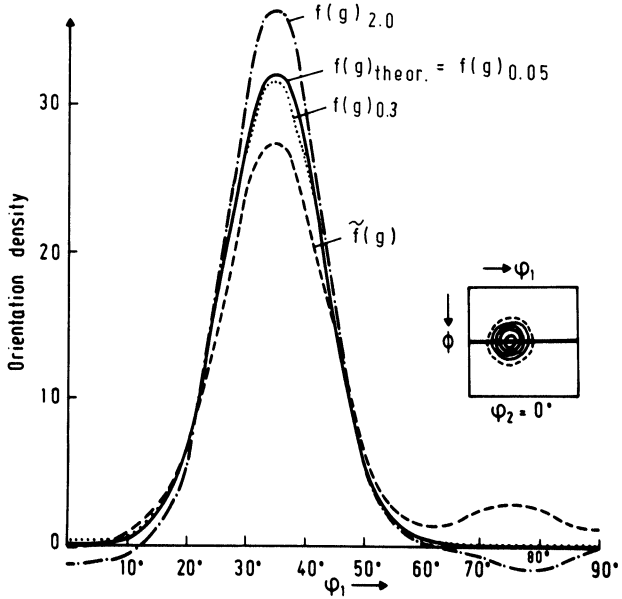


FIGURE 8 Section of the ODFs obtained theoretically and by application of the zero-range method with different definitions $P_i^0$ of the "physical zero".

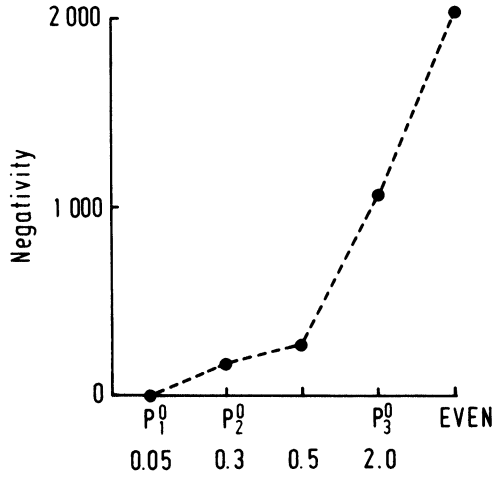


FIGURE 9 Negativity values of the calculated ODFs as a function of the definition of zero $P_i^0$.

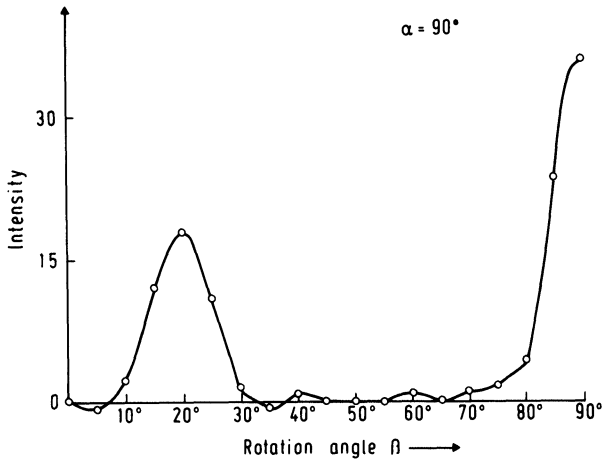


FIGURE 10 Section $\alpha = 90°$ of the (111) pole figure of an ideal texture $g = \{100\}\langle 112\rangle$ $\omega_0 = 6°$, $L = 22$ showing truncation error.

with $\omega_0 = 12°$. A comparison of the theoretical coefficients with the ones obtained by the zero-range method can be made according to Figure 11. It is seen that the "experimental" error reduces the accuracy of the obtained odd coefficients strongly. The corresponding section of the ODF is shown in Figure 12.

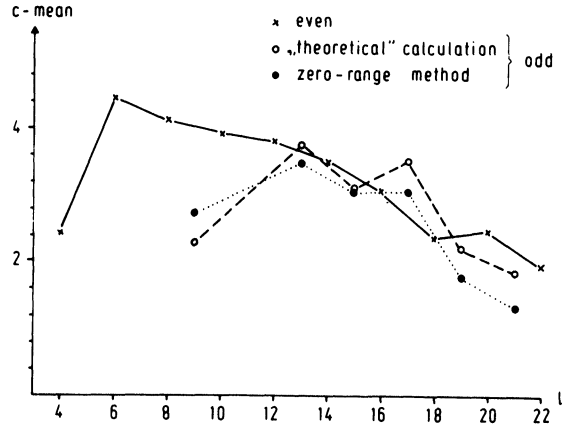


FIGURE 11 Mean values of the coefficients $C_l^{\mu\nu}$ over $\mu$ and $\nu$ for a theoretical texture $g = \{110\}\langle 112\rangle$, $\omega_0 = 6°$, $L = 22$.

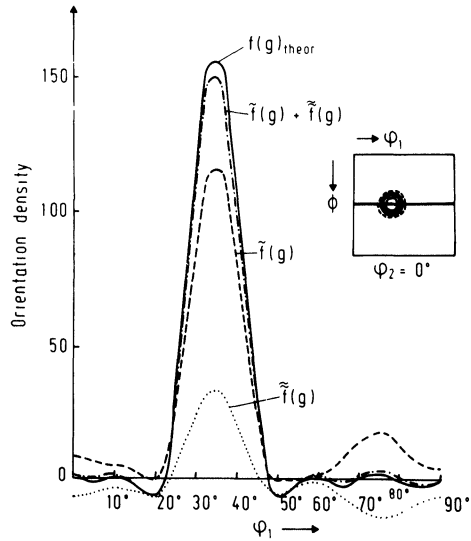


FIGURE 12 Sections of the ODF of a theoretical texture $g\{110\}\langle 112\rangle$, $\omega_0 = 6°$, $L = 22$. The zero-range was defined with $P^0 = 0.05$.

## AN EXPERIMENTAL TEXTURE

The influence of the definition of "physical zero" on the obtained complete ODF was also tested with an experimental texture, i.e. the rolling texture of a low carbon steel which was determined by neutron diffraction. Four pole figures (200) (110) (211) and (310)

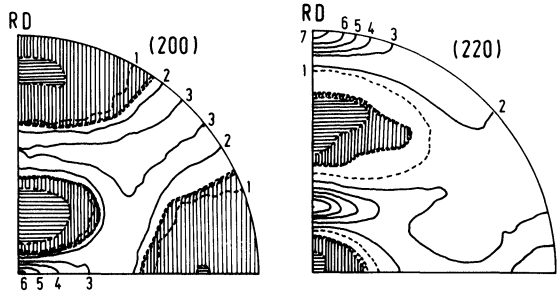


FIGURE 13 The zero-ranges in the pole figures (200) and (220) of a cold rolled low carbon steel according to three different definitions.

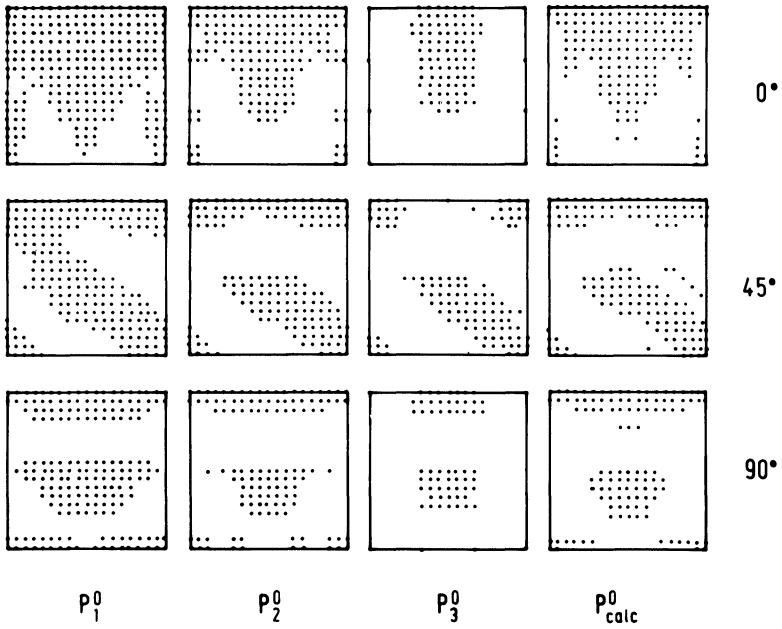


FIGURE 14 The zero-ranges (white) and non-zero-ranges (points) in the orientation space according to the three definitions $P_i^0$ of the zero-ranges in the pole figures including the one obtained from recalculated pole figures.

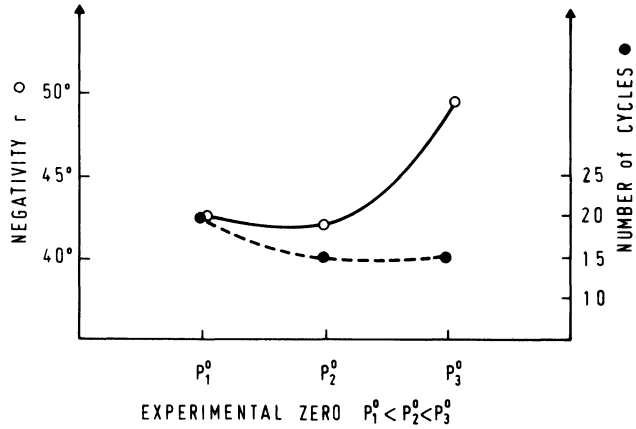


FIGURE 15 The number of cycles $n$ needed in order to solve Eq. (26) and the negativity parameter $r$ as a function of $P_i^0$ defining the zero-range.

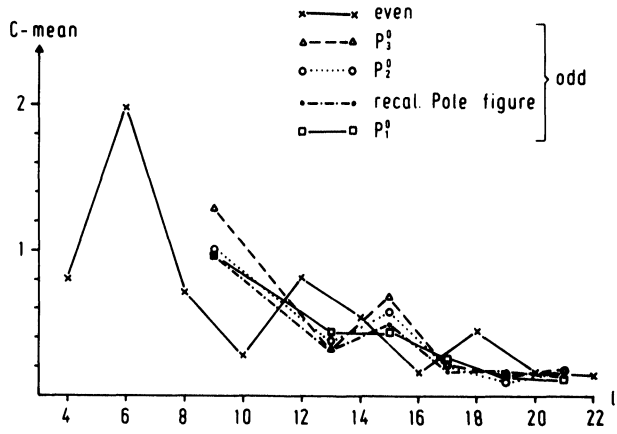


FIGURE 16 Mean values over $\mu$ and $\nu$ of the coefficients $C_l^{\mu\nu}$ obtained with different definitions of the zero-range.

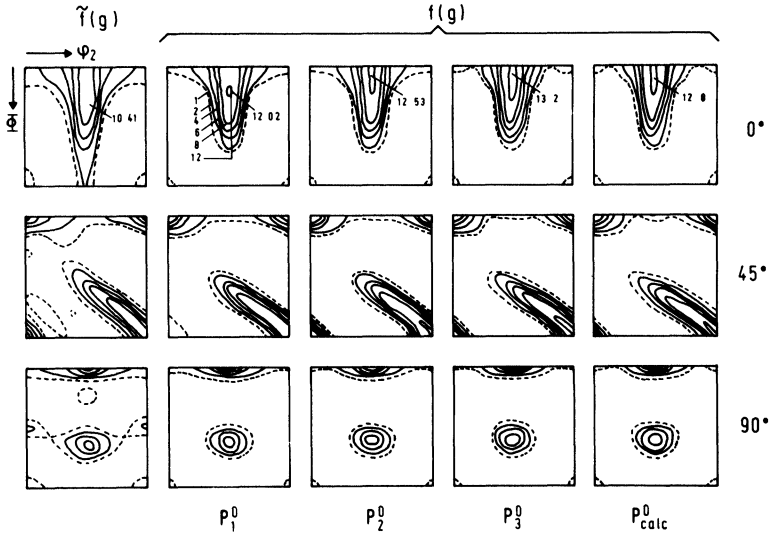


FIGURE 17 The reduced ODF $\tilde{f}(g)$ of a low carbon steel obtained from four complete pole figures measured by neutron diffraction and the complete ODFs obtained with different definitions of the zero-range including a calculation from recalculated pole figures.

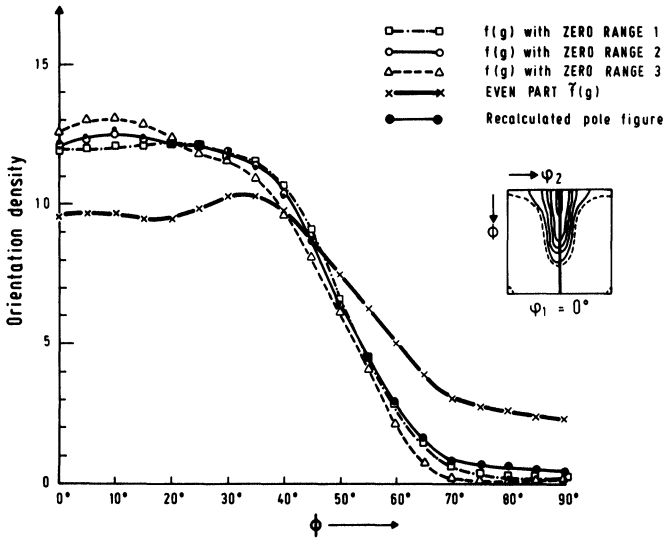


FIGURE 18 Sections at $\varphi_1 = 0°$, $\varphi_2 = 45°$ of the ODFs of Figure 17.

were measured in steps of $2.5^0 \times 3.6^0$. Zero values $P_1^0$, $P_2^0$, $P_3^0$ were assumed which lead to the zero-ranges in the (200) and (220) pole figures shown in Figure 13. Meaningful zero-ranges were not obtained in the other two pole figures. Hence, the zero-ranges in the orientation space were determined from these two pole figures. They are shown in Figure 14 together with the one obtained from recalculated pole figures. The number of cycles needed in order to solve Eq. (26) is shown in Figure 15. It is a measure for a sufficiently large zero-range. The mean values of the so obtained coefficients are shown in Fig. 16. The ODFs themselves are represented in Figure 17. Although the zero-ranges are quite different using the different definitions $P_i^0$, the obtained ODFs are very similar. This is also seen in Figure 18 which contains sections through the ODFs at $\varphi_1 = 0°$, $\varphi_2 = 45°$. The negativity values $r$ according to Eq. (33) are also shown in Figure 15 which thus serves to determine the optimum choice of the zero-range. Figures 14 to 17 also show a calculation carried out with a zero-range determined from recalculated pole figures.

## CONCLUSIONS

It has been shown by an example using a theoretical texture that the zero-range method defined in Eq. (19) yields a good approximation $\tilde{\tilde{f}}_{L_1}(g)$ to the "indeterminable" part $\tilde{\tilde{f}}(g)$ of the ODF if a sufficiently large zero-range is available in which Eq. (18) holds. The larger the zero-range the better is the solvability of Eq. (26) and the better is the extrapolation of the approximation function $\tilde{\tilde{f}}_{L_1}$ into the non-zero-range.

The extension of the zero-range must be defined by some appropriately chosen "physical" zero value $P^0$. The choice of $P^0$ has two consequences: the larger $P^0$ the larger is the zero-range and hence the better is the solvability of Eq. (26) which improves the result, the larger $P^0$ the larger are, however, also the deviations from Eq. (18) and hence the errors in $\tilde{\tilde{f}}(g)$ introduced in Eq. (19) which deteriorates the result. Hence, an optimum choice of $P^0$ has to be made in order to obtain optimum results.

Independent of a correct definition of the zero-range, i.e. the validity of Eq. (18), the error of the reduced ODF $\tilde{f}(g)$ fully enters Eq. (19) and hence Eq. (26) and its solution. This error is composed of the experimental error of the pole figures and the truncation error in the determinable part $\tilde{f}(g)$ of the ODF.

Although the choice of the "physical zero" value $P^0$ in an experimental example influences the size of the zero-range considerably, the influence on the final result of the complete ODF is rather limited such that the exact choice of $P^0$, compared with other experimental errors, is not a critical quantity.

A good estimation of the zero-range can be made in the recalculated pole figures using the maximum negative value in these pole figures as a physically meaningful "zero". This choice is well adapted to all errors, experimental and truncational, which enter the calculation of the odd coefficients. Furthermore the use of recalculated pole figures allows one to determine a larger part of the zero-range than with the use of incomplete experimental pole figures. It is thus especially indicated in this latter case.

## References

1. Bechler-Ferry, E., Bunge, H. J. and Esling, C. (1981). Proc. 6th Intern. Conf. on Textures of Materials ICOTOM 6 Tokyo, 1359–1369.

2. Bunge, H. J. (1965). *Z. Metallkunde* **56,** 827–874.
3. Bunge, H. J. (1982). Texture Analysis in Materials Science. Butterworths, London.
4. Bunge, H. J. and Esling, C. (1979). *C. R. Acad. Sc. Paris* **B289,** 163–164.
5. Bunge, H. J. and Esling, C. (1979). *Journal de physique, lettres* **40,** 627–628.
6. Bunge, H. J. and Esling, C. (1981). *J. Appl. Cryst.* **14,** 253–255.
7. Bunge, H. J. and Esling, C. (1985). *Acta Cryst.* **A41,** 59–67.
8. Bunge, H. J., Esling, C. and Muller, J. (1980). *J. Appl. Cryst.* **13,** 544–554.
9. Bunge, H. J., Esling, C. and Muller, J. (1981). *Acta Cryst.* **A37,** 889–899.
10. Esling, C., Bechler-Ferry, E. and Bunge, H. J. (1981). *C. R. Acad. Sc. Paris II,* **292,** 159–162.
11. Esling, C., Bechler-Ferry, E. and Bunge, H. J. (1981). *Journal de physique, lettres* **42,** 141–144.
12. Esling, C. and Bunge, H. J. (1981). Proc. 6th Intern. Conf. on Textures of Materials ICOTOM 6 Tokyo 1426–1435.
13. Esling, C., Muller, J. and Bunge, H. J. (1982). *J. Physique* **43,** 189–195.
14. Imhof, J. (1977). *Z. Metallkde* **68,** 38–43.
15. Lee, H. P. (1985). Texturanalyse unter der Anwendung der Nullbereichsmethode, Thesis Clausthal.
16. Lee, H. P., Welch, P. I., Esling, C. and Bunge, H. J. (1984). Proc. 7th Intern. Conf. on Textures of Materials ICOTOM 7. Nordwijkerhout 799–803.
17. Matthies, S. (1979). *Phys. Stat. Sol.* **B92,** K135–138.
18. Matthies, S. (1982). Aktuelle Probleme der quantitativen Texturanalyse. Zentralinstitut für Kernforschung Rossendorf.
19. Roe, R. J. (1965). *J. Appl. Phys.* **36,** 2024–2031.
20. Ruer, D., Baro, R. (1977). *Adv. X-Ray Anal.* **20,** 187–200. Plenum Press, New York.
21. Wassermann, G., and Grewen, J. (1962). Texturen metallischer Werkstoffe, Springer-Verlag Berlin.
22. Wenk, H. R., and Wilde, W. R. (1972). Geophysical Monograph Series 16.
23. Williams, R. O. (1968). *Trans Met. Soc. AIME* **242,** 104–115.